Proc. Natl. Acad. Sci. USA
Vol. 96, pp. 3200–3205, March 1999
Neurobiology

Functional repair of motor endplates after botulinum neurotoxin type A poisoning: Biphasic switch of synaptic activity between nerve sprouts and their parent terminals

ANTON DE PAIVA*†, FRÉDÉRIC A. MEUNIER*†, JORDI MOLGÓ‡, K. ROGER AOKI§, AND J. OLIVER DOLLY*¶

*Department of Biochemistry, Imperial College of Science, Technology, and Medicine, London SW7 2AY, United Kingdom; ‡Laboratoire de Neurobiologie Cellulaire et Moléculaire, Centre National de la Recherche Scientifique, Gif-sur-Yvette, 91198 Cedex, France; and §Allergan, 2525 Dupont Drive, Irvine, CA 92715

Edited by Richard Winyu Tsien, Stanford University School of Medicine, Stanford, CA, and approved December 30, 1998 (received for review October 13, 1998)

ABSTRACT **Blockade of acetylcholine release by botulinum neurotoxin type A at the neuromuscular junction induces the formation of an extensive network of nerve-terminal sprouts. By repeated *in vivo* imaging of *N*-(3-triethyl ammonium propyl)-4-(4-(dibutylamino)styryl) pyridinium dibromide uptake into identified nerve endings of the mouse sternomastoid muscle after a single intramuscular injection of the toxin, inhibition of stimulated uptake of the dye at the terminals was detected within a few days, together with an increase in staining of the newly formed sprouts. After 28 days, when nerve stimulation again elicited muscle contraction, regulated vesicle recycling occurred only in the sprouts [shown to contain certain soluble *N*-ethylmaleimide-sensitive factor attachment proteins (SNAREs) and to abut acetylcholine receptors] and not at the parent terminals. Therefore, only these sprouts could be responsible for nerve–muscle transmission at this time. However, a second, distinct phase of the rehabilitation process followed with a return of vesicle turnover to the original terminals, accompanied by an elimination of the by then superfluous sprouts. This extension and later removal of "functional" sprouts indicate their fundamental importance in the repair of paralyzed endplates, a finding with ramifications for the vital process of nerve regeneration.**

The ability of nerve endings at the neuromuscular junction to sprout after the potent blockade of neurotransmission by botulinum neurotoxin type A (BoTx/A) is a striking example of synaptic plasticity (1–4). Although significant progress already has been made in identifying the factors triggering such outgrowth (see ref. 5), as well as that induced on, for example, partial denervation by nerve crush (1, 6), the significance of endplate remodeling in the intricate series of interactions between presynaptic and postsynaptic cells during recovery of transmission at paralyzed synapses has yet to be shown. The selective blockade of the regulated exocytosis of acetylcholine (ACh) by BoTx/A after its intracellular proteolytic cleavage of synaptosomal-associated protein with a molecular mass of 25 kDa (SNAP-25; ref. 7 and 8) causes an unique and long-term eradication of synaptic activity, while, advantageously, avoiding removal of the nerve endings (9, 10). Despite the extent of the paralysis induced by this toxin, recovery of neurotransmission does occur eventually, as manifested in animal experiments (2, 11–13) and in the clinical treatment of dystonias involving involuntary movement of certain skeletal muscles (see ref. 14). Although BoTx/A is known to promote nerve sprouting, it has remained unclear what the precise contribution, if any, these newly formed outgrowths make to the recovery from this initially dramatic, but ultimately temporary, paralysis.

Limitations encountered in earlier studies on this fundamentally important question originated from the need to employ conventional histological techniques *in vitro* to excised tissues. These limitations have been overcome in our study by using high-sensitivity computer-controlled video microscopy to perform repeated imaging of fluorescently labeled nerve endings in living mice. The viewing of identified nerve endings before and after injection of BoTx/A into surgically exposed sternomastoid muscle of the anesthetized mouse allowed monitoring of alterations in both the morphology and loci of synaptic-vesicle turnover in the same individual terminals during the entire period of intoxication and recovery. The resultant data, when taken together with immunodetection of synaptic proteins essential for neurotransmission in the presynaptic processes and nicotinic ACh receptors (nAChR) in the adjacent postsynaptic membrane, show that the sprouts, and not the originally poisoned terminals, are the only sites undergoing depolarization-dependent vesicle turnover at the onset of the recovery of nerve-stimulated muscle contraction. Additionally, a much slower but complete restoration of functionality to the parent terminals was shown to occur eventually, accompanied by elimination of the by then superfluous sprouts. It has, therefore, been concluded that the sprouts are formed to release ACh and induce electrical activity that is thought to be essential for the dynamic interplay between motor nerves and nonneuronal cells that aid the implementation of a full recovery from paralysis.

MATERIALS AND METHODS

Repeated Visualization of Endplates in Living Mice. Tyler's Ordinary mice (15–20 g) of either sex were anesthetized deeply with 10 ml/kg i.p. anesthetic (0.079 mg/ml fentanyl citrate/2.5 mg/ml fluanisone/0.5 mg/ml midazolam). The superficial ventral musculature of the neck was exposed (15), and the right sternomastoid muscle was lifted onto a flattened wire. Nerve endings were stained for 5 min with either 5 μM 4-(4-diethyl aminostyryl)-*N*-methylpyridinium iodide (4-di-2-ASP; Molecular Probes) alone in aerated Krebs–Ringer solution [(in mM) 118 NaCl/4.69 KCl/1.18 $MgSO_4$/1.18 KH_2PO_4/11.7 glucose/

The publication costs of this article were defrayed in part by page charge payment. This article must therefore be hereby marked "*advertisement*" in accordance with 18 U.S.C. §1734 solely to indicate this fact.

PNAS is available online at www.pnas.org.

This paper was submitted directly (Track II) to the *Proceedings* office. Abbreviations: 4-di-2-ASP, 4-(4-diethyl aminostyryl)-*N*-methylpyridinium iodide; ACh, acetylcholine; BoTx/A, botulinum neurotoxin type A; d*n*, day *n* (after toxin injection); FITC, fluorescein isothiocyanate; FM1-43, *N*-(3-triethyl ammonium propyl)-4-(4-(dibutylamino)styryl) pyridinium dibromide; LAL, levator auris longus muscle; nAChR, nicotinic ACh receptors; SNARE, soluble *N*-ethylmaleimide-sensitive factor attachment protein receptor.

†A.d.P. and F.A.M. contributed equally to this work.
¶To whom reprint requests should be addressed. e-mail: o.dolly@ic.ac.uk.

23.8 $NaHCO_3$/2.52 $CaCl_2$, pH 7.4; ref 16] or in high K^+ Krebs–Ringer solution (with 60 mM KCl and 58 mM NaCl) containing both 5 μM 4-di-2-ASP and 4 μM *N*-(3-triethyl ammonium propyl)-4-(4-(dibutylamino)styryl) pyridinium dibromide (FM1-43; Molecular Probes). Then, in both instances, the wound was washed extensively with normal Krebs–Ringer solution for 3 min. All buffers were run through a 0.2-μm filter before use. After placing an 8-mm diameter circular coverslip mounted on a second wire over the endplate region, each mouse was positioned under a Zeiss Axioskop fixed-stage microscope equipped with epifluorescence. Staining with 4-di-2-ASP was visualized with an fluorescein isothiocyanate (FITC)-type narrow band-pass filter block (450- to 490-nm excitation λ; 515- to 565-nm emission λ), and dual labeling with 4-di-2-ASP and FM1-43 was detected by using the aforementioned filter and a long-pass rhodamine-type block (524- to 556-nm excitation λ; $\geq$590-nm emission λ), respectively. To prevent photodamage to tissues, the excitation intensity was minimized, and images were recorded with an intensified CCD video camera (Jai 758, Datacell, Yateley, U.K.) and IMAGE PRO PLUS (version 3.0; Datacell) imaging software. The same single terminals were observed repeatedly over a number of weeks (15) through Zeiss $\times$20/0.50 and $\times$40/0.75 water-immersion objectives. For dual staining, the same camera-intensifier gain and black levels were used for each sequential viewing of the endplates. Images of three to five selected endplates from each mouse were captured as individual sequences of 8 or 16 frames, which were then averaged. After image acquisition, BoTx/A-hemagglutinin complex (List Biological Laboratories, Campbell, CA; 0.5 pg per 20 g of body weight at a concentration of 0.25 pg/μl) was injected into the sternomastoid muscle with a microsyringe $\approx$2 mm from the endplate region; the time of injection was considered the day-0 time point (d0). The incision was closed with four or five sutures. Toxin-treated nerve endings were later visualized a second and third time by repeating the above procedures. When analyzing endocytosis with FM1-43 at the nerve terminals and their outgrowths, artificial color was added to the stored images, and views of 4-di-2-ASP and FM1-43 stained terminals were overlaid; then, the luminance levels in each color channel were quantified by calculating the average intensity values of a band of lines encompassing the entire sprout or terminal with IMAGE PRO PLUS. Intensity integrations and statistical analysis were performed after exporting the data to EXCEL 97 (Microsoft). Sprout length, number, and branching also were quantified with IMAGE PRO PLUS. Only after all data had been extracted were the image γ levels adjusted for presentation purposes; this adjustment was performed batchwise in PHOTOSHOP (version 5.0), and the same adjustments were applied to all images.

***In Vivo* Evaluation of FM1-43 Release from Sprouts.** Exocytosis from the sprouts was monitored by measuring diminution of stimulation-induced FM1-43 staining at all time points (but not on every muscle). Nerve processes on the surgically exposed sternomastoid muscle, which had already been labeled with this dye as described above, were reimaged after a 10-min depolarization in 60 mM K^+ Krebs–Ringer solution. During the acquisition of images of resting sprouts preloaded with FM1-43 and those stimulated to measure release, it was ensured that fluorescence-excitation intensity as well as camera-intensifier gain and black levels were standardized. This standardization allowed direct comparison of the illumination intensities and evaluation of the extent of activity-induced destaining. It should be noted that in these experiments, FM1-43 fluorescence was visualized through an FITC-type block.

Immunolabeling and Laser Scanning Confocal Microscopy. Control and BoTx/A-poisoned mouse sternomastoid and levator auris longus muscles (LAL) were treated *in situ* in cervically dislocated animals with 240 units/ml type I collagenase (Sigma) and 0.2 mg/ml trypsin inhibitor in Krebs–Ringer solution at 37°C for 30 min. Muscles were then washed and fixed with 4% (wt/vol) paraformaldehyde in 0.1 M PBS (pH 7.4) for 10 min before excision. Dissected preparations were kept in the fixative solution for 1.5 h and washed in PBS. Sternomastoid muscle fibers were separated by gentle teasing in the same buffer before processing for immunostaining. The very thin LAL were not teased apart before staining. A 20-min incubation of the fibers in PBS supplemented with 3% (vol/vol) goat serum and 0.4% (vol/vol) Triton X-100 at room temperature quenched nonspecific protein binding and made the membranes permeable. This incubation was followed by an overnight incubation at 4°C in the same buffer containing a 1:100 dilution of the primary antibodies raised against recombinant glutathione *S*-transferase-SNAP-25, a synthetic peptide comprising residues 33–94 of human synaptobrevin II (17), or specific for the 68-kDa isoform of neurofilament (Sigma). After several washes in PBS containing 0.4% (vol/vol) Triton X-100 for 1 h at room temperature, the samples were incubated for 2 h with the FITC-conjugated secondary antibodies (Sigma; anti-rabbit IgG for SNAP-25 or synaptobrevin and anti-mouse IgG for neurofilament) at room temperature in the dark. For localizing endplates, postsynaptic nAChRs were dual-stained with rhodamine-conjugated α-bungarotoxin. Samples were then mounted with Fluoprep (BioMerieux, Marcy l'étoile, France) and viewed with a Bio-Rad 600 Confocal system on a Nikon Optiphot-2 microscope.

Intoxication, Excision, and FM1-43 Staining of Mouse LAL. BoTx/A (0.5 pg) was injected into the vicinity of the LAL (13) in female Swiss mice ($\approx$20 g). After cervical dislocation of both control mice and those injected with toxin, the nerve-muscle preparations were superfused continuously with oxygenated Krebs–Ringer solution [(in mM) 151 NaCl/5 KCl/1 $MgCl_2$/2 $CaCl_2$/11 glucose/5 Hepes, pH 7.4] during excision. The tissues either were immersed in this buffer containing 4 μM FM1-43 or were stimulated in high K^+ Krebs–Ringer solution (with 60 mM K^+ and 58 mM Na^+) for 5 min before extensive washing (30 min) in normal Krebs–Ringer solution and imaging with a Sarastro 2000 laser confocal system (Molecular Dynamics) controlled by IMAGESPACE (version 3.10) and a Nikon Optiphot-2. Fluorescence was excited with the 488-nm line of an argon ion laser and viewed through a $\times$40/0.55 water-immersion objective. The pinhole aperture was set to 100 μm, and images were digitized at an 8-bit resolution into a 512 $\times$ 512 array. To equate the intensity of FM1-43 staining in different preparations accurately, laser illumination, photomultiplier gain, and other acquisition variables were standardized. Series of optical sections were averaged, and a "look-through" projection was generated. Images from each experiment were processed identically before quantitation by outlining the nerve endings and determining the mean fluorescence (F) per square micrometer. Mean background fluorescence (B) per square micrometer was also measured in the surrounding muscle fibers. The index of the composite levels of FM1-43 uptake then was calculated as $(F - B)/B$.

RESULTS

Functionality of Mouse Motor Endplates Switches to Synapses Newly Formed by Nerve-Terminal Sprouts Induced by BoTx/A. The elegant procedure designed in the laboratory of Lichtman *et al.* (15, 18), allowing the repeated visualization of single identified terminals in the sternomastoid muscle of living mice, was adapted to trace the precise pattern of endplate remodeling that ensues the blockade of ACh release by BoTx/A. After surgical exposure of the muscle, a computer-controlled and intensified CCD video camera was used to capture epifluorescence images of representative terminals and their toxin-elicited outgrowths stained with the fluorescent vital dye 4-di-2-ASP (19) and the exoendocytotic marker FM1-43 (20–22). Sequential imaging allowed direct morpho-

logical comparison of the exact same terminals immediately before and after toxin injection and determination of stimulated vesicle turnover within these remodeled nerve endings. To allow a direct correlation between these visualized features and the time at which neurotransmission resumes in previously paralyzed muscle, an evaluation of nerve-induced muscle contraction after supramaximal electrical stimulation of the spinal accessory nerve innervating the sternomastoid fibers was also made when imaging these nerve endings in living mice.

Before FM1-43 was used as a marker of exoendocytosis, two criteria had to be established. First, because these terminals cannot be preloaded with FM1-43 (20), it was essential to confirm that the measurement of stimulated endocytosis reflects the toxin-induced blockade of exocytosis (23). Control nerve terminals on the sternomastoid muscle, depolarized with 60 mM K^+ in the presence of FM1-43 and then extensively washed, were labeled 3- to 4-fold more effectively than nonstimulated control endplates (data not shown, but see Fig. 3 for equivalent experiments in mouse LAL) and those stimulated after poisoning 3 days earlier with BoTx/A (Fig. 1*a*). This result shows that BoTx/A-treatment of mammalian nerve endings leads to an impairment of regulated vesicle endocytosis—as well as exocytosis—and confirms findings made earlier in frog terminals (24). Second, the feasibility of dual labeling nerve endings with FM1-43 and 4-di-2-ASP had to be determined for this *in vivo* imaging procedure. On staining the nerve endings with either or both of the dyes, it was found that, although FM1-43 is viewed commonly as a green fluorescence (20), its detection was also possible in the red channel via a long-pass rhodamine-type block because of the relatively broad excitation and emission spectra of this dye. In contrast, 4-di-2-ASP was seen (at the low excitation intensities used here) only through an FITC-type filter; therefore, both dyes could be viewed simultaneously.

Imaging the individually unique nerve endings on the sternomastoid fibers immediately before injection of BoTx/A (d0) indicated colocalization of 4-di-2-ASP and activity-dependent staining with FM1-43 (Fig. 1 *a*, *b*, *e*, and *f*). From d3 to d7, activity-dependent uptake of FM1-43 in these same original terminals was found to be diminished (see Fig. 1*h*). At this time, electrical stimulation of the spinal accessory nerve failed to elicit visible muscle contraction, despite the obvious twitching of the uninjected cleidomastoideus and clavotrapezius fibers also innervated by this nerve. Remodeling of these poisoned terminals became apparent at d4; short ($\approx$4.3-μm) nerve sprouts appeared, extending beyond the original endplate (see Table 1). Subsequent reimaging of these endplates and comparison with their original morphologies over the first 4 weeks indicated further dramatic increases in the number, length (by d28, the average sprout length was $\approx$70.2 μm), and complexity of these processes (Table 1). Over this same period, FM1-43 labeling in the original terminals was maintained at a low level, but, by d7, depolarization-dependent uptake of this dye became evident within the outgrowths (Fig. 1*h*). Confocal imaging of nerve endings in fibers injected 9 days earlier and dual-stained for one or the other of the two soluble *N*-ethylmaleimide-sensitive factor attachment protein proteins (SNAREs) plus nAChRs indicated the presence of SNAP-25 and synaptobrevin within these outgrowths (Fig. 2 *b* and *e*) but only a minor reorganization of the postsynaptic nAChRs. However, a general increase in background binding of α-bungarotoxin was evident, perhaps indicating an up-regulation in ectopic nAChR synthesis. It should be noted that the anti-SNAP-25 IgG used here does not distinguish between the BoTx/A-cleaved form and the intact protein.

At later times (d14 and d28), FM1-43 staining remained at the low residual level in the original terminals but continued to increase in the extending sprouts (Fig. 1 *b* and *h*). Indeed, by d28, when twitch of the sternomastoid muscle was elicited on direct electrical stimulation of the nerve for the first time after BoTx/A-poisoning, the sprouts exhibited long expanses of activity-dependent uptake of FM1-43-labeled vesicles, particularly toward their endings (Fig. 1*b*). If such loaded sprouts (Fig. 1*c*) were stimulated with 60 mM K^+ for 10 min before reimaging, a marked destaining was observed (Fig. 1*d*), thereby establishing that both synaptic vesicle uptake and release occur in these processes. In confirmation of the functionality of the sprouts, confocal imaging of these nerve endings immunostained for SNAP-25, synaptobrevin, and neurofilament indicated the presence of all three along the entire lengths of the extended sprouts as well as at the original terminals (Fig. 2 *c*, *f*, and *g*). Within these sprouted processes, the staining patterns of the individual SNAREs were similar to those seen in the control endplates (Fig. 2 *a* and *d*). Moreover, at d18–d28, a clear reorganization of the postsynaptic nAChRs had now also taken place as evidenced by the distinguishable patches of α-bungarotoxin staining that were visible abutting the sprouts, particularly toward their extremities (Fig. 2 *c*, *f*, and *g*). Collectively, these data show that not only is the machinery in place to mediate neurotransmission at the sprouts but, also, stimulated uptake and release of FM1-43 were occurring only within these newly formed sprouts and not the original terminals at the time of the first return of detectable nerve-induced muscle twitch. Thus, it is apparent that neurotransmission at this stage is mediated by "functional" synapses formed between the terminal sprouts and the muscle fibers, and these can, at least temporarily, play the role of the parent terminals in muscle paralyzed by BoTx/A.

An Eventual Loss of Endocytotic Activity from the Sprouts and Their Elimination Coincides with the Return of Synaptic Function to the Original Nerve Endings. At the onset of the recovery of muscle poisoned with BoTx/A, as seen at d28, the amplitude of the endplate potential (2, 13) triggered via the sprouts must be above the threshold for action-potential generation in at least a significant portion of the muscle fibers. However, electromyographic recordings in BoTx/A-injected mouse peroneus and soleus muscles (25) showed that the signal amplitude was at first subnormal, even when these muscles were no longer paralyzed, and a normal value returned only $\approx$50 days later. Furthermore, the composite level of FM1-43 staining at d42, although greater than the low level measured at d3 (Fig. 3), was still significantly lower than in control terminals (Fig. 3). Thus, after the initial synaptic reorganization highlighted in the present study, further alterations must occur to facilitate the eventual full return of nerve–muscle transmission to the level that existed before BoTx/A poisoning.

In vivo observations of endplates on the sternomastoid muscle indicated that, despite the recovery from paralysis at d28, further augmentation of the sprouts ensued for a further 2 weeks (Table 1) as did global FM1-43 uptake in the remodeled neuronal network of the LAL (Fig. 3). An eventual cessation in their expansion was visualized commencing at d42, and morphometric analysis over the next 3 weeks indicated a slight drop in the number of sprouts and the degree of secondary branching (Table 1). Also, during this period (d42–d63), a gradual but marked diminution in activity-dependent staining by FM1-43 was detected *in vivo* in the sprouts, especially toward their extremities (Fig. 1 *e*, *f*, and *h*). However, concomitant with this recession of vesicle turnover in the outgrowths, a marked increase in FM1-43 staining in the original endplates was recorded (Fig. 1 *e*, *f*, and *h*), indicating a return of synaptic activity. Global levels of FM1-43 uptake in the LAL measured after confocal imaging also continued to increase over this period (Fig. 3). As FM1-43 uptake at the original endplate increased further over the next 4 weeks (Fig. 1*h*), the previously extensive sprouts receded (Fig. 1*f*), and 3 months after BoTx/A injection, the endplates had regained morphologies and patterns of depolarization-stimulated

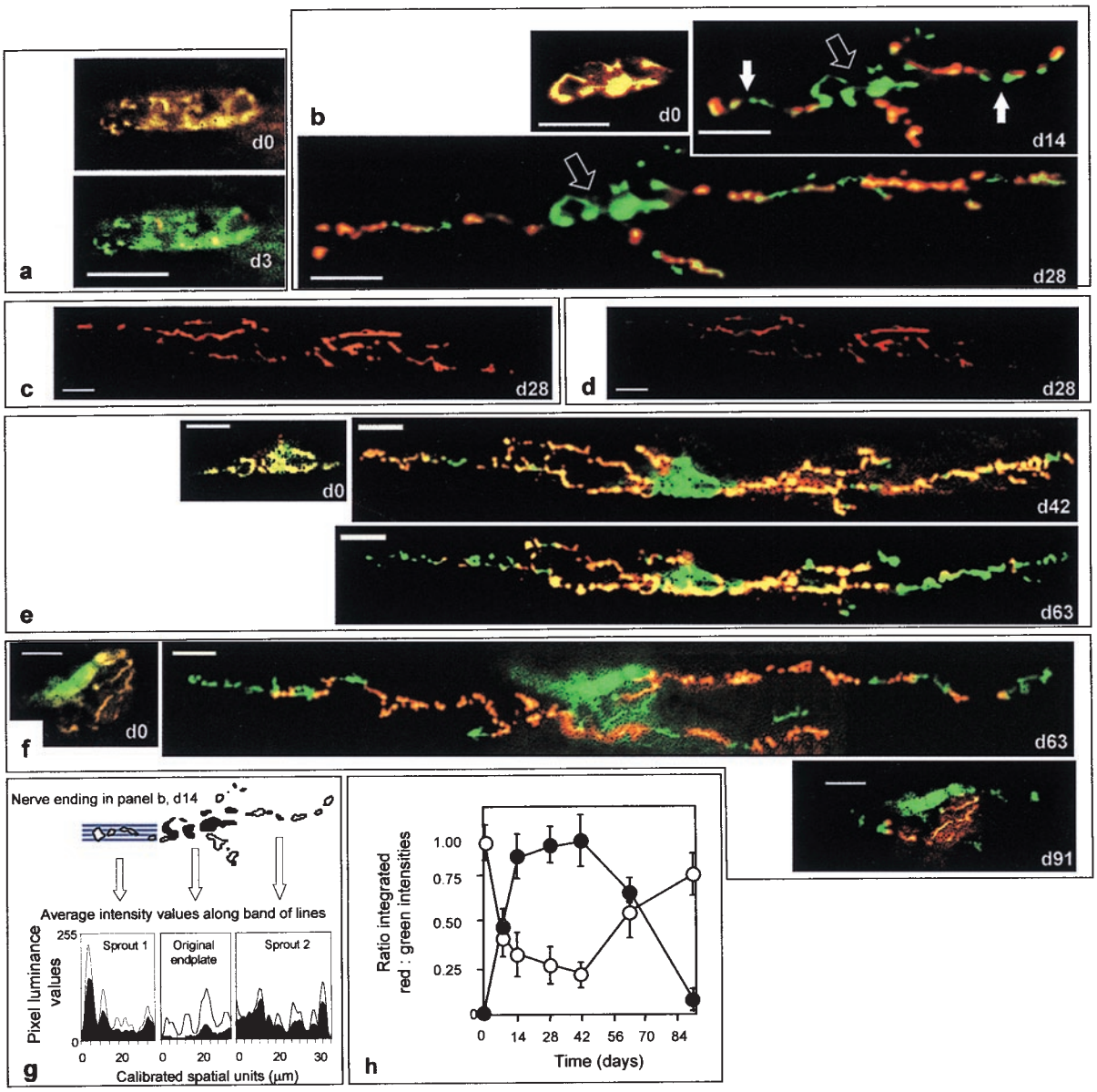

FIG. 1. Repeated *in vivo* visualization of FM1-43 uptake into nerve endings on the mouse sternomastoid muscle (taken before and after BoTx/A-poisoning) indicated a transient switch in the locus of stimulation-dependent vesicular uptake and release between the nerve terminals and their toxin-induced sprouts. (*a*, *b*, *e*, and *f*) At d0, before BoTx/A injection, FM1-43 (red) uptake was seen in the nerve terminals also stained with 4-di-2-ASP (green), and their overlap appears as yellow. (*a*, d3) Imaging at d3 indicated a dramatic diminution in depolarization-induced FM1-43 uptake. Although staining of the original terminals (*b*, open arrows) remained suppressed, FM1-43 endocytosis became apparent in the sprouts (*b*, closed arrows), after their appearance and extension (*b*; d14 and d28). In a separate experiment, FM1-43-loaded sprouts (*c*) at d28 were destained visibly on depolarization (*d*), establishing that they also can mediate stimulated exocytosis. On further extension (*e*; up to d42) the sprouts continued to be labeled with FM1-43, but imaging at d63 and thereafter indicated that uptake recovered in the parent terminals, while such staining in the sprouts began to decline preceding their retraction (*e* and *f*; d63). (*f*; d91) By d91, FM1-43 uptake at the original endplate closely resembled that recorded immediately before injection. Luminance levels were quantified for both 4-di-2-ASP and FM1-43 staining in the original endplates and sprouts, as illustrated, for example, at d14 (*b*); filled arrows in that image pinpoint two of the four sprouts present. (*g*) The average pixel-intensity values calculated from bands of lines (depicted schematically for sprout 1) are plotted for red (filled curve) and green (open curve) channels for these two processes and the original terminals. (*h*) The integrated red and green intensity values for all sprouts (closed circles) and their parent terminals (open circles) obtained in this manner were averaged ±SEM (from 11–16 endplates in three or four mice at each time point), and their ratios were plotted for the entire time course. *a*, *b*, *e* and *f* show repeated visualizations of the same endplates with each series having been obtained from different animals. (Bars = 20 μm.)

FM1-43 staining in the sternomastoid muscle (Fig. 1*f*)—as well as total levels of dye uptake within terminals in the LAL (Fig. 3)—that were indistinguishable from those visualized before poisoning.

DISCUSSION

A multidisciplinary approach allowed us to dissect the intriguing adaptation of the neuromuscular junction that allows survival and, eventually, complete recovery from BoTx-induced neuroparalysis. On the resumption of nerve-induced muscle twitch detectable 4 weeks after intoxication, an extensive network of sprouts containing SNAP-25, synaptobrevin, and neurofilament had developed. As already shown elsewhere, the newly formed processes contain a number of other proteins essential for neurotransmission: synaptotagmin II and synaptophysin (13), voltage-sensitive Na^+ and Ca^{2+} channels for action-potential conduction and nerve-evoked transmitter

Table 1. BoTx/A-induced terminal sprouts visualized with 4-di-2ASP in living mice

Sprout criteria	d2	d4	d7	d14	d28	d42	d63	d91
No. of sprouts	0	1.2 ± 0.2	1.6 ± 0.3	2.6 ± 0.7	3.9 ± 1.3	4.1 ± 0.9	3.9 ± 0.5	2.1 ± 0.3
Average sprout length, μm	0	4.3 ± 5.8	9.9 ± 5.2	28.4 ± 9.6	70.2 ± 17.7	150.6 ± 20.1	133.6 ± 18.9	3.9 ± 0.1
No. of branches	0	1.7 ± 0.5	2.5 ± 0.9	6.8 ± 0.2	11.6 ± 3.4	16.2 ± 3.4	13.8 ± 4.9	3.6 ± 0.6

Note that within the population of endplates viewed on the ventral surface of the sternomastoid muscle, <10% of the terminals elicited very small or in rare instances (≈1%), no obvious sprouts. Nevertheless, when performing statistical calculations on these morphological parameters, measurements from all terminals were included. Furthermore, as well as the terminal sprouts described here, outgrowths from the last node of Ranvier also were detected occasionally but not traced in this study. Values are means of 10–12 endplates from three mice ± SEM.

release, and Ca^{2+}-dependent K^+ channels that can control the latter process (2). Moreover, we show here that, on formation, these sprouts acquire the ability to mediate stimulated vesicle turnover and, at the onset of recovery of nerve-induced muscle twitch, exoendocytosis occurs only within these sprouts and not in the parent terminals. When taken together with the aggregation of nAChRs (see also refs. 2 and 26) in the postsynaptic membrane seen in apposition to the sprouts at this time, our results establish that the site of nerve-induced muscle stimulation had shifted from the original endplates to the sprouts. Such clustering of nAChRs, predominantly abutting the distal extremities of the newly formed sprouts, accords with the release of neural agrin that is known to occur from motor-nerve growth cones during programmed and induced plasticity at the neuromuscular junction (27). Although this agrin-mediated cascade of events has not yet been investigated in BoTx/A-poisoned tissues, the prominent clustering of nAChRs beneath the sprouts suggests a role for agrin in stabilizing the nAChR clusters at the newly formed sprouts.

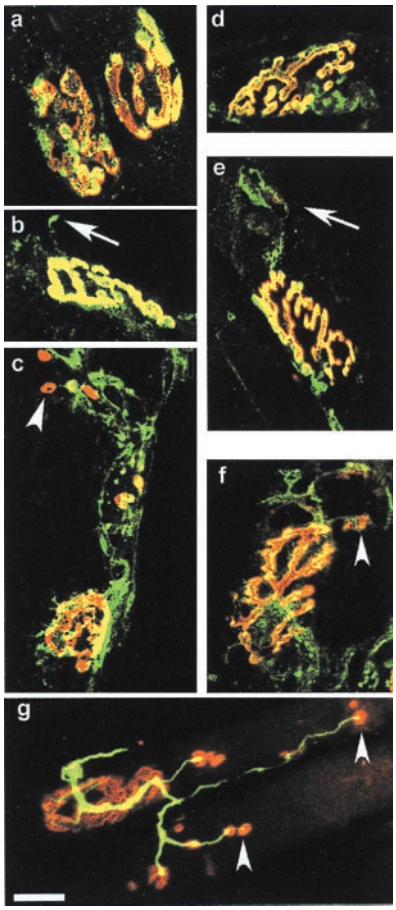

FIG. 2. Control and BoTx/A-treated endplates dual-labeled with rhodamine-conjugated α-bungarotoxin and FITC-conjugated secondary IgGs reactive with antibodies bound to synaptobrevin, SNAP-25, or neurofilament. On control sternomastoid muscle fibers, synaptobrevin (*a*) and SNAP-25 (*d*) staining was colocalized within the areas occupied by the nAChRs; unlike synaptobrevin, SNAP-25 was also detected in the axons. At d9, both synaptobrevin (*b*) and SNAP-25 (*e*) were detected in the sprouts extending beyond the area containing nAChRs (arrows). By d28, sprouts containing the v-SNARE (*c*) and t-SNARE (*f*) had extended to form a complicated network. (*c* and *f*, arrowheads) At this time, clusters of nAChRs were detected abutting these sprouts. (*g*) This clustering of nAChRs was also seen in mouse LAL injected with BoTx/A 18 days earlier and dual-stained with antineurofilament IgG. (Bars = 20 μm.)

The original terminals remain unable to undergo measurable exoendocytosis until almost 2 months after injection of BoTx/A, a period of time which is significantly longer than the turnover rate of SNAP-25, at least when measured in the optic tract and superior colliculi (28) and cultured PC12 cells (29). Although these cells are specialized and have substantial dissimilarities from the motor-nerve endings examined in the present study, possible explanations for this apparent inconsistency are (*i*) that the active toxin remains compartmentalized within the original terminals and cleaves any newly synthesized SNAP-25; (*ii*) that nonfunctional, truncated SNAP-25 persists in the original terminals; and (*iii*) that the proteolysis of SNAP-25 by the toxin induces a cascade of events culminating in a widespread perturbation of the original terminal that can be overcome only by a long-term remodeling process. Although it is not possible, at this stage, to distinguish between any of these scenarios, future experiments could include antibodies capable of distinguishing newly synthesized intact and BoTx/A-cleaved SNAP-25 to help establish a basis for this prolonged blockade of ACh release at the original nerve endings seen here.

Retraction of the Sprouts and Return of Functionality to the Original Terminals. Previous studies on excised tissues have yielded conflicting results regarding the long-term presence of

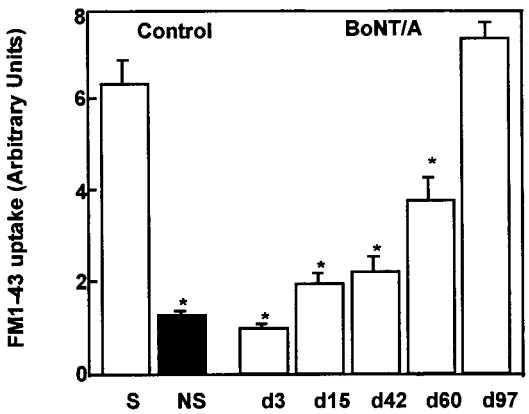

FIG. 3. Quantitation of activity-dependent uptake of FM1-43 in excised living motor-nerve terminals from control and mouse LAL injected with BoTx/A. The first two bars represent measured fluorescence levels in stimulated (S) and nonstimulated (NS) terminals of control muscle. The next five bars show the progressive increase of depolarization-dependent uptake of FM1-43 into the terminals and sprouts in previously paralyzed tissue. The control level is reached only at d97. Values presented represent the mean index of FM1-43 uptake ±SEM of 100–200 measurements performed on two to six neuromuscular preparations. *, $P < 0.01$; Student's *t* test.

sprouts after recovery from BoTx/A-induced paralysis. Although some reported the regression of such sprouts in mouse (12, 25), rat (30), and human (31) muscles, others provided no evidence for the elimination of sprouts on recovery from BoTx/A poisoning (32, 33). Also, in patients treated for blepharospasm with BoTx/A, some sprouts were detectable many months after injection (34). Such inconsistencies have probably arisen for two major reasons. First, in the case of the latter study, apart from the obvious difficulties in precisely comparing time courses in human and mice, patients had been treated with multiple (2–18) injections of toxin before muscle biopsies were stained and visualized, thereby resulting in a cumulative effect and a more complicated pattern of remodeling. Second, the use of classical cytochemical techniques on excised muscle precluded a precise comparison being made of the same terminals before and after intoxication. In contrast, the *in vivo* imaging technique employed here allowed sequential visualization of identified terminals before and after BoTx/A injection and, combined with extensive statistical analysis of all endplates visualized, has facilitated an accurate determination of the long-term pattern of this sprouting response. Indeed, we have shown that after a brief supplementary augmentation of the functional processes subsequent to the onset of recovery of nerve-induced muscle twitch, an eventual cessation of their outgrowth ensues and, on the eventual return of exoendocytosis to the original terminals, the sprouts gradually lose their ability to perform endocytosis for FM1-43 and, shortly thereafter, start to regress. The competition that arises between the recovered original terminals and the sprouts apparently results in the ultimate retraction of the sprouts.

Importance of Nerve-Terminal Sprouts in the Recovery of Neurotransmission After Paralysis. The pattern of sprouting elicited after BoTx/A-induced blockade of ACh release is not a precise emulation of neuronal remodeling seen after all types of injury in the peripheral and central nervous systems. For instance, when a peripheral nerve is crushed, motor axons and endplates distal to the injury degenerate and the muscles become denervated (35), unlike BoTx/A-poisoned terminals, which persist despite their loss of activity. However, an important similarity does exist: sprouts—both collateral and terminal—also are formed after nerve crush (1), resulting in polyneuronal innervation until these surplus synapses are eliminated eventually (35). The functionality of terminal sprouts and the overlap in plastic reactions after both nerve injury and BoTx/A poisoning highlight the importance of synaptic remodeling in instigating the eventual recovery of neurotransmission after paralysis. The emergence of sprouts via rapid extension of the terminal membranes is triggered by paralysis-induced changes in the levels of intrinsic as well as extrinsic neurotrophic factors and proteases. For example, sprouting can be stimulated by ciliary neurotrophic factor (36) and insulin-like growth factors I and II (37). Electrical activity stimulates the presynaptic and/or postsynaptic production of neurotrophins and raises the sensitivity of neurons to these factors (38, 39). In accordance with such interplay, the muscle activity initially evoked solely via the sprouts in the absence of any exoendocytotic activity within the parent poisoned terminals may in turn induce a late phase of the remodeling process culminating in the complete functional repair of the original terminals.

This work is sponsored by Allergan. F.A.M. was supported in part by Direction des Recherches Etudes et Techniques and by European Commission Biotechnology Program Grant B104CT965119. J.M. was supported by Direction des Systèmes de Forces et de la Prospective.

1. Brown, M. C., Holland, R. L. & Hopkins, W. G. (1981) *Annu. Rev. Neurosci.* **4,** 17–42.
2. Angaut-Petit, D., Molgó, J., Comella, J. X., Faille, L. & Tabti, N. (1990) *Neuroscience* **37,** 799–808.
3. Comella, J. X., Molgó, J. & Faille, L. (1993) *Neurosci. Lett.* **153,** 61–64.
4. Tsukahara, N. (1981) *Annu. Rev. Neurosci.* **4,** 351–379.
5. Caroni, P. (1997) *BioEssays* **19,** 767–775.
6. Rich, M. M. & Lichtman, J. W. (1989) *J. Neurosci.* **9,** 1781–1805.
7. Schiavo, G., Santucci, A., DasGupta, B. R., Mehta, P. P., Jontes, J., Benfenati, F., Wilson, M. C. & Montecucco, C. (1993) *FEBS Lett.* **335,** 99–103.
8. Blasi, J., Chapman, E. R., Link, E., Binz, T., Yamasaki, S., DeCamilli, P., Sudhöf, T. C., Niemann, H. & Jahn, R. (1993) *Nature (London)* **365,** 160–163.
9. Duchen, L. W. (1971) *J. Neurol. Sci.* **14,** 47–60.
10. Molgó, J., Comella, J. X. & Angaut-Petit, D. (1990) *J. Physiol. (Paris)* **84,** 152–166.
11. Duchen, L. W. & Strich, S. J. (1968) *Q. J. Exp. Physiol.* **53,** 84–89.
12. Holland, R. L. & Brown, M. C. (1981) *Neuroscience* **6,** 1167–1179.
13. Juzans, P., Comella, J. X., Molgó, J., Faille, L. & Angaut-Petit, D. (1996) *Neuromuscul. Disord.* **6,** 177–185.
14. Cava, T. J. (1995) *Eur. J. Neurol.* **2,** 57–60.
15. Lichtman, J. W., Magrassi, L. & Purves, D. (1987) *J. Neurosci.* **7,** 1215–1222.
16. de Paiva, A., Poulain, B., Lawrence, G. W., Shone, C. C., Tauc, L. & Dolly, J. O. (1993) *J. Biol. Chem.* **268,** 20838–20844.
17. Foran, P., Lawrence, G. W., Shone, C. C., Foster, K. A. & Dolly, J. O. (1996) *Biochemistry* **35,** 2630–2636.
18. Balice-Gordon, R. J. & Lichtman, J. W. (1990) *J. Neurosci.* **10,** 894–908.
19. Magrassi, L., Purves, D. & Lichtman, J. W. (1987) *J. Neurosci.* **7,** 1207–1214.
20. Betz, W. J. & Bewick, G. S. (1992) *Science* **255,** 200–203.
21. Betz, W. J., Mao, F. & Smith, C. B. (1996) *Curr. Opin. Neurobiol.* **6,** 365–371.
22. Ribchester, R. R., Mao, F. & Betz, W. J. (1994) *Proc. R. Soc. London Ser. B* **255,** 61–66.
23. Valtorta, F., Fesce, R., Grohovaz, F., Haimann, C., Hurbut, W. P., Lezzi, N., Torri Tarelli, F., Villa, A. & Ceccarelli, B. (1990) *Neuroscience* **35,** 477–489.
24. Henkel, A. W., Simpson, L. L., Ridge, R. M. A. P. & Betz, W. J. (1996) *J. Neurosci.* **16,** 3960–3967.
25. Tian, W. H., Festoff, B. W., Blot, S., Diaz, J. & Hantai, D. (1995) *Synapse* **20,** 24–32.
26. Yee, W. C. & Pestronk, A. (1987) *J. Neurosci.* **7,** 2019–2024.
27. Ruegg, M. A. & Bixby, J. L. (1998) *Trends Neurosci.* **21,** 22–27.
28. Loewy, A., Liu, W.-S., Baitinger, C. & Willard, M. B. (1991) *J. Neurosci.* **11,** 3412–3421.
29. Lane, S. R. & Liu, Y. C. (1997) *J. Neurochem.* **69,** 1864–1869.
30. Hassan, S. M., Jennekens, F. G. I., Wieneke, G. & Veldman, H. (1994) *Muscle Nerve* **17,** 623–631.
31. Chou, S. M. (1992) in *Skeletal Muscle Pathology*, eds. Mastaglia, F. L. & Walton, J. N. (Churchill Livingstone, London), pp. 599–637.
32. Duchen, L. W. (1970) *J. Neurol. Neurosurg. Psychiatry* **33,** 40–54.
33. Porter, J. D., Strebeck, S. & Capra, N. F. (1991) *Arch. Opthalmol.* **109,** 396–404.
34. Alderson, K., Holds, J. B. & Anderson, R. L. (1991) *Neurology* **41,** 1800–1805.
35. Herrera, A. A. (1997) in *Advances on Organ Biology—The Synapse: In Development, Health, and Disease*, eds. Festoff, B. W., Hantai, D. & Citron, B. A. (JAI, London), Vol. 2, pp. 29–53.
36. Gurney, M. E., Yamamoto, H. & Kwon, Y. (1992) *J. Neurosci.* **12,** 3241–3247.
37. Caroni, P., Schneider, C., Kiefer, M. C. & Zapf, J. (1994) *J. Cell Biol.* **125,** 893–902.
38. Thoenen, H. (1995) *Science* **270,** 593–598.
39. McAllister, A. K., Katz, L. C. & Lo, D. C. (1996) *Neuron* **17,** 1057–1064.